Chem Soc Rev

Cite this: DOI: 10.1039/c1cs15172j

www.rsc.org/csr

CRITICAL REVIEW

Graphene-based semiconductor photocatalysts

Quanjun Xiang,[a] Jiaguo Yu*[a] and Mietek Jaroniec*[b]

Received 24th June 2011
DOI: 10.1039/c1cs15172j

Graphene, a single layer of graphite, possesses a unique two-dimensional structure, high conductivity, superior electron mobility and extremely high specific surface area, and can be produced on a large scale at low cost. Thus, it has been regarded as an important component for making various functional composite materials. Especially, graphene-based semiconductor photocatalysts have attracted extensive attention because of their usefulness in environmental and energy applications. This *critical review* summarizes the recent progress in the design and fabrication of graphene-based semiconductor photocatalysts *via* various strategies including *in situ* growth, solution mixing, hydrothermal and/or solvothermal methods. Furthermore, the photocatalytic properties of the resulting graphene-based composite systems are also discussed in relation to the environmental and energy applications such as photocatalytic degradation of pollutants, photocatalytic hydrogen generation and photocatalytic disinfection. This *critical review* ends with a summary and some perspectives on the challenges and new directions in this emerging area of research (158 references).

1. Introduction

Graphene, a single layer of sp^2-bonded carbon atoms tightly packed into a two-dimensional honeycomb structure, has attracted a lot of attention since its discovery in 2004,[1] due to its outstanding mechanical, thermal, optical, and electrical properties. Especially, graphene possesses a high thermal conductivity ($\sim$5000 W m^{-1} K^{-1}), offers an excellent mobility of charge carriers at room temperature (200 000 cm^2 V^{-1} s^{-1}), and exhibits an extremely high theoretical specific surface area ($\sim$2600 m^2 g^{-1}).[2–4] To date, various methods have been developed for the preparation of graphene, including micromechanical exfoliation, epitaxial growth, chemical and electrochemical reduction of graphite oxide and bottom-up organic synthesis.[3–9] Among these methods, the reduction of exfoliated

[a] *State Key Laboratory of Advanced Technology for Material Synthesis and Processing, Wuhan University of Technology, Luoshi Road 122#, Wuhan 430070, P. R. China. E-mail: jiaguoyu@yahoo.com; Fax: +86-27-87879468; Tel: +86-27-87871029*
[b] *Department of Chemistry, Kent State University, Kent, Ohio 44242, USA. E-mail: jaroniec@kent.edu; Fax: +1-330-672 3816; Tel: +1-330-672 3970*

Quanjun Xiang

Quanjun Xiang received his BE from the Department of Materials Science and Engineering at Henan Polytechnic University in 2007. He is currently a PhD candidate under the supervision of Prof. Jiaguo Yu from the State Key Laboratory of Advanced Technology for Materials Synthesis and Processing at Wuhan University of Technology. His current research interests are focused on the design and synthesis of photocatalytic materials for energy and environmental applications.

Jiaguo Yu

Jiaguo Yu received his BS and MS in chemistry from Huazhong Normal University and Xi'an Jiaotong University, respectively; his PhD in Materials Science in 2000 from Wuhan University of Technology. In 2000, he became a Professor at Wuhan University of Technology. He was a postdoctoral fellow at the Chinese University of Hong Kong from 2001 to 2004, a visiting scientist from 2005 to 2006 at University of Bristol, a visiting scholar from 2007 to 2008 at University of Texas at Austin. His research interests include semiconductor photocatalysis, photocatalytic hydrogen production, dye-sensitized solar cells, adsorption, CO_2 sequestration, graphene, nanocarbons and related nanomaterials.

graphene oxide (GO) was proven to be an effective and reliable method to produce graphene nanosheets owing to low cost and massive scalability.[10] Moreover, the surface properties of graphene can be adjusted *via* chemical modification, which offers tremendous opportunities for the development of functionalized graphene-based materials.[8,11] Such graphene-based materials show unique electronic and optical properties and good biocompatibility, which make these materials attractive for many potential applications including energy storage,[12] catalysis,[13] biosensors,[14] molecular imaging[15] and drug delivery.[16] Recently, functionalized graphene-based semiconductor photocatalysts have attracted a lot of attention due to their good electron conductivity, large specific surface area and high adsorption.[17–22]

Since the discovery of the photocatalytic splitting of water on TiO_2 electrodes by Fujishima and Honda in 1972,[23] a significant progress has been made in the area of highly active oxide semiconductor photocatalysts because of their applicability in solar energy conversion and environmental protection. Some semiconductors (*e.g.*, ZnO, WO_3, CdS, Bi_2WO_4 and BiOCl, *etc.*) can act as photocatalysts for light-induced chemical transformations due to their unique electronic structure composed of a filled valence band (VB) and an empty conduction band (CB). When a photon with energy of $h\nu$ matches or exceeds the band gap energy (E_g) of the semiconductor, an electron in the VB is excited into the CB, leaving a positive hole in the VB. The photogenerated holes and electrons play a very important role in pollutant degradation and photocatalytic disinfection, and solar energy conversion including hydrogen production and solar photovoltaics, respectively. However, the photogenerated electrons and holes in the excited states are unstable and can easily recombine, dissipating the input energy as heat, which results in low efficiency of photocatalysis.[24–27]

During the past decade, a variety of strategies have been employed to improve the photocatalytic performance of semiconductor photocatalysts, for example, *via* suitable textural design,[28–33] doping,[34–37] noble metal loading[38–40] and forming semiconductor composites.[41,42] In particular, numerous attempts have been made to combine graphene with semiconductor photocatalysts to enhance their photocatalytic performance.[19–21,43–48] For example, Kamat and co-workers[19,20,49,50] produced GO–TiO_2 nanocrystalline composites by sonicating dispersed TiO_2 nanoparticles and GO in ethanol and demonstrated the feasibility of using graphene as an electron-transfer medium in the graphene/TiO_2 composite photocatalysts. This pioneering work has stimulated an extensive research on the preparation, modification, and application of graphene-based semiconductor photocatalysts. Zhang *et al.*[21] reported graphene–P25 TiO_2 composites synthesized under hydrothermal conditions that exhibited an enhanced photocatalytic activity for the degradation of methylene blue in aqueous solutions. Ng *et al.*[43] demonstrated a great performance of the $BiVO_4$–GO composite photocatalyst in the visible light range for water splitting. Since many important findings have been reported on the graphene-based semiconductor photocatalysts during the past few years, we believe that a comprehensive review on this subject is timely to promote further developments in this exciting area of research. This review is focused on the recent progress in the design, fabrication, modification and applications of graphene-based semiconductor photocatalysts, and provides some invigorating perspectives on the future developments.

Mietek Jaroniec

Mietek Jaroniec received his MS and PhD from M. Curie-Sklodowska University, Poland, in 1972 and 1976, respectively. Since 1991 has been a Professor of Chemistry at Kent State University, Kent, Ohio (USA). Before joining Kent State he was a Professor of Chemistry at M. Curie-Sklodowska University, Poland. His research interests revolve primarily around interdisciplinary topics of interfacial chemistry, chemical separations, and chemistry of materials, including physical adsorption at the gas/solid and liquid/solid interfaces, gas and liquid chromatography, adsorbents and catalysts. At Kent State he has established a vigorous research program in the area of ordered nanoporous materials such as ordered mesoporous silicas, organosilicas, inorganic oxides and carbons, focusing on their synthesis and environmental and energy-related applications.

2. Preparation

2.1 Synthesis of graphene

Since the first report on graphene obtained by manual mechanical cleavage of graphite with a Scotch tape,[1] a wide range of techniques for the synthesis of this material have been reported.[3] In general, these techniques can be divided into "bottom-up" and "top-down" methods. In the bottom-up methods, graphene is synthesized from atoms or molecules *via* chemical reactions. Some typical examples are epitaxial growth on single-crystal SiC and chemical vapor deposition (CVD) on metal foil surfaces.[5,6,51–53] These resulting graphene films can be easily transferred to polymer substrates by etching away the metal supports. However, these methods are not widely used because of their complexity, limited scaling-up and high cost of the precious metal substrates. To date, high-quality graphene with a well-defined molecular structure was usually prepared by top-down methods such as chemical exfoliation of graphite,[54,55] thermal exfoliation[56] and electrostatic deposition.[57] Especially, the most widely used technique is chemical reduction of GO as shown in Fig. 1, which is usually conducted by Hummers' method.[58] According to this method, the reduced GO is prepared by exfoliating graphite oxide, obtained by oxidation of natural graphite powder with strong chemical oxidants, such as HNO_3, $KMnO_4$ and H_2SO_4. The resulting GO product is usually purified by centrifugation, washing, and dialysis to remove some aggregates and various inorganic impurities such as residual ions and acids. More importantly, the exfoliated GO sheets usually possess a rich assortment of oxygen-containing groups, such as carboxylic,

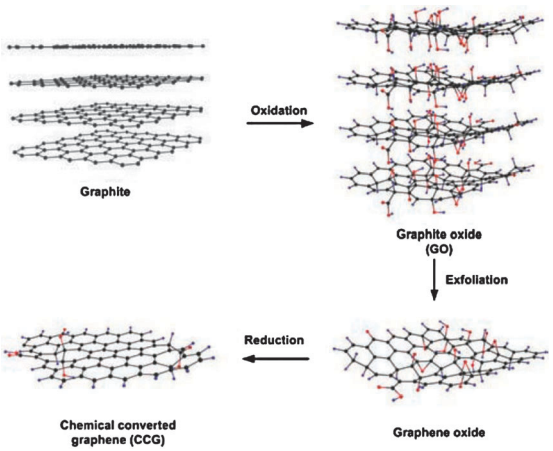

Fig. 1 Preparation of graphene by chemical reduction of graphene oxide synthesized by Hummers' method. Reprinted with permission from ref. 9. Copyright 2011, Wiley-VCH.

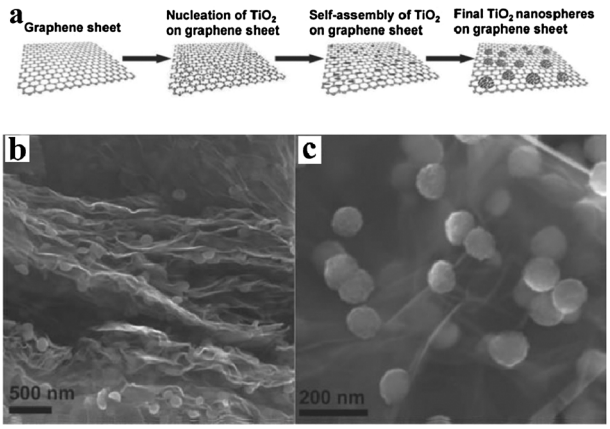

Fig. 2 (a) Schematic illustration of the template-free self-assembly strategy for the preparation of mesoporous TiO_2 nanospheres/graphene composites. (b) Side-view and (c) top-view SEM images of as-prepared mesoporous anatase TiO_2 nanospheres/graphene composites. Reprinted with permission from ref. 105. Copyright 2011, Wiley-VCH.

hydroxyl, and epoxide functional groups. The presence of oxygen functionalities in GO allows interactions with the cations and provides reactive sites for the nucleation and growth of nanoparticles, which results in the rapid growth of various graphene-based composites. Moreover, the functional GO can be reduced to graphene with partial restoration of the sp^2-hybridized network by thermal,[59] chemical,[60] electrochemical,[61] photothermal,[62] photocatalytic,[63] sonochemical,[64] and microwave reduction methods.[65]

2.2 Preparation of graphene-based semiconductor photocatalysts

A variety of semiconductor photocatalysts have been used for the synthesis of graphene-based composites and/or functional GO. They mainly include metal oxides (*e.g.* TiO_2,[18,21,66–74] ZnO,[48,75–80] SnO_2,[81–83] Cu_2O,[84] Fe_2O_3,[85] NiO,[86] MnO_2[87] and ZrO_2[88]), salts (*e.g.* ZnS,[89] CdS,[89–93] CdSe,[94] Bi_2WO_6,[95] $BiVO_4$,[43] $Sr_2Ta_2O_7$,[96] $ZnFe_2O_4$,[97] $InNbO_4$[98] and γ-Bi_2MoO_6[99]), metal-free polymers (*e.g.* graphitic carbon nitride[100,101]) and silver/silver halides (Ag/AgCl,[102,103] and Ag/AgBr[103]). The widely used preparation methods are *in situ* growth, solution mixing, hydrothermal and/or solvothermal method. The following paragraphs will give a more detailed description of the available synthesis routes.

2.2.1 ***In situ* growth strategy.** The direct growth strategy is widely used to prepare graphene based-metal compound composites. The most common precursors of graphene and metal compound are functional GO and metal salts, respectively. Usually, the salt is mixed with GO and then converted to the corresponding oxide, forming a GO/metal compound composite. After reduction of GO, graphene based-metal compound composites were produced. For example, Sn^{2+} or Ti^{3+} ions were added into a functional GO dispersion solution and converted to SnO_2 or TiO_2 nanoparticles at low temperatures. In this process GO was reduced to graphene by $SnCl_2$ or $TiCl_3$.[81] The growth of SnO_2 and TiO_2 nanocrystals of different morphologies on the reduced GO sheets was attributed to the different reduction abilities and hydrolysis rates of Sn^{2+} and Ti^{3+}, respectively. A graphene–ZnO composite was synthesized analogously. Zn^{2+} ions were adsorbed on graphene oxide sheets and converted into ZnO nanoparticles with the addition of NaOH and $NaBH_4$ under drying in air at 150 °C.[48] After reduction of graphene oxide, a graphene/ZnO composite photocatalyst was produced. In this composite, the size of ZnO nanoparticles formed on graphene sheets was in the range of 10–20 nm with a narrow particle size distribution. Lambert *et al.*[104] also reported the *in situ* synthesis of composites comprised of flower-like anatase TiO_2–graphene oxide by the hydrolysis of TiF_4 in the presence of aqueous dispersions of GO. In this case, when the concentration of graphene oxide was sufficiently high and stirring was off, a long-range ordered assemblies of TiO_2-GO sheets were obtained. Li *et al.*[105] developed a direct growth of uniform mesoporous anatase TiO_2 nanospheres on graphene sheets by a template-free self-assembly process (see Fig. 2). They used titanium sulfate and functional graphene sheets as the starting materials. The epoxy and hydroxyl functional groups on graphene sheets acted as heterogeneous nucleation sites by anchoring anatase nanoparticles, which resulted in the formation of well-dispersed mesoporous anatase TiO_2 nanospheres on the graphene sheets. Interestingly, the oriented attachment of some very small primary TiO_2 nanoparticles facilitated the formation of a single-crystal-like microstructure within a single nanosphere during the assembly process of these nanospheres on graphene sheets. Further extensions of the direct growth strategy were used to prepare a variety of graphene based-composites. For example, Wang *et al.*[106] used anionic sulfate surfactants to assist the stabilization of graphene in aqueous solutions and to facilitate the self-assembly of *in situ* grown nanocrystalline TiO_2, rutile and anatase, with graphene. Park and co-authors[107] prepared TiO_2 nanoparticles coated with graphite oxide layers by the spontaneous exfoliation and reorganization of graphite oxides in aqueous slurry without using any chemical reagents under ambient conditions. Du *et al.*[108] also prepared the hierarchically ordered macro-mesoporous TiO_2–graphene composite film. They used a confinement self-assembly method to produce the hierarchically

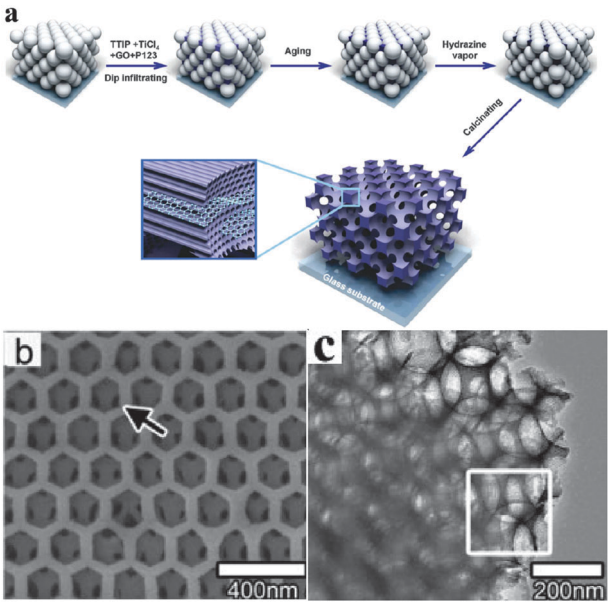

Fig. 3 (a) Schematic illustration of the preparation of the ordered macro-mesoporous TiO_2–graphene composite film by *in situ* reduction of graphene oxide added into the self-assembly system. (b) SEM and (c) TEM images of the macro-mesoporous TiO_2–graphene composite film. Reprinted with permission from ref. 108. Copyright 2011, American Chemical Society.

ordered porous titania films with two-dimensional hexagonal mesostructures and well-interconnected periodic macropores. Then, graphene was incorporated into the resulting titania framework by *in situ* reduction of graphene oxide added into the self-assembled system (see Fig. 3).

The *in situ* growth strategy can avoid the agglomeration of the semiconductor nanoparticles on the graphene sheets. Zhu *et al.*[109] reported a one-pot method for water-phase synthesis of high-quality graphene/TiO_2 composite nanosheets using $TiCl_3$ as a reducing agent and the titania precursor. Similarly, a graphene/CdS composite was also prepared by a one-step method using GO and $Cd(CH_3COO)_2{\cdot}2H_2O$ in DMSO.[90] During this one-step reaction, H_2S released from DMSO acted as both the reducing agent of GO and the sulfide source. Thus, the reduction of GO and the deposition of CdS on the graphene sheets occurred simultaneously, resulting in a uniform and tight distribution of CdS nanoparticles on graphene sheets. The size of the CdS nanoparticles in the composite was around 10 nm (see Fig. 4). Chen *et al.*[110] reported the fabrication of graphene sheets-wrapped anatase TiO_2 hollow particles. The electroactive egg-like TiO_2 hollow particles were first synthesized, and then these particles were functionalized with aminopropyltrieth-oxysilane to obtain a positively-charged surface. Next, the negatively charged GO sheets were linked to these functionalized TiO_2 hollow particles *via* simple electrostatic interaction. Finally, the GO sheets were reduced to graphene sheets by thermal treatment under an inert atmosphere, leading to the formation of graphene–TiO_2 composites.

2.2.2 Solution mixing method. Solution mixing has been widely used to fabricate graphene/semiconductor composite photocatalysts. For example, TiO_2 particles and GO colloids

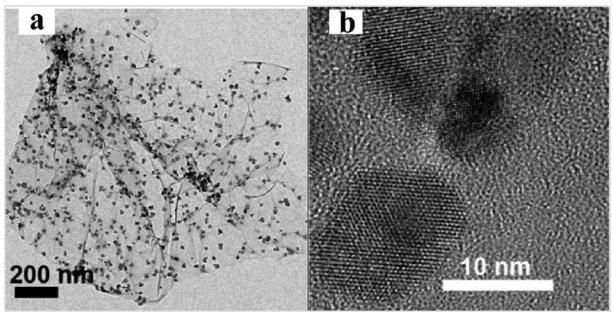

Fig. 4 (a) TEM and (b) high-resolution TEM images of the graphene/CdS composite prepared by a solvothermal *in situ* growth method. Reprinted with permission from ref. 90. Copyright 2010, Wiley-VCH.

have been mixed ultrasonically, followed by ultraviolet (UV)-assisted photocatalytic reduction of GO to yield TiO_2/graphene composites.[111] Akhavan and Ghaderi[112] used a similar strategy to prepare the TiO_2/graphene composite thin film. Paek *et al.*[113] synthesized the SnO_2 sol by hydrolysis of $SnCl_4$ with NaOH, and then the prepared graphene dispersion was mixed with the sol in ethylene glycol to form the SnO_2/graphene composite. Mukherji *et al.*[96] prepared nitrogen doped $Sr_2Ta_2O_7$ coupled with graphene sheets by mixing the graphene oxide dispersion and $Sr_2Ta_2O_{7-x}N_x$, followed by reduction of graphene oxide to graphene under xenon lamp irradiation. Zhu *et al.*[103] used the water/oil system to produce GO enwrapped Ag/AgX (X = Br, Cl) composites. They added aqueous solutions of GO and $AgNO_3$ to chloroform solution of CTAB or CTAC under magnetic stirring at room temperature to produce Ag/AgX/GO hybrid composites (Fig. 5). Considering graphene's large network of sp^2 hybridized carbon, this material can tend to form strong π–π bonds with other graphite-like materials. Sun *et al.*[100] synthesized a composite polymeric photocatalyst graphene/graphitic carbon nitride by a combined solution mixing–chemical reduction strategy. Graphitic carbon nitride was deposited on the surface of GO sheets to form a layered composite by polymerizing melamine molecules adsorbed on GO due to the π–π interaction of aromatic structures between graphene oxide and graphitic carbon nitride. Similarly, Geng *et al.*[94] mixed graphene oxide sheets and the CdSe nanoparticles modified with pyridine to produce graphene–CdSe quantum dots composites. They thought that pyridine ligands could provide π–π interactions for the assembly of CdSe nanoparticles capped with pyridine on GO sheets.

2.2.3 Hydrothermal/solvothermal method. The hydrothermal/solvothermal process, one of the traditional methods for crystal growth of semiconductors, is another effective method for the preparation of semiconductor composites with graphene. In this process, semiconductor nanoparticles or their precursors are loaded on the graphene oxide sheets, which are reduced to graphene. For example, Fu and Wang[97] synthesized the $ZnFe_2O_4$–graphene composite photocatalyst with different graphene contents by a one-step hydrothermal method in ethanol-aqueous solution. They used $Zn(NO_3)_2{\cdot}6H_2O$ and $Fe(NO_3)_3{\cdot}9H_2O$ as precursors of $ZnFe_2O_4$, and GO as a source of graphene sheets. During the hydrothermal

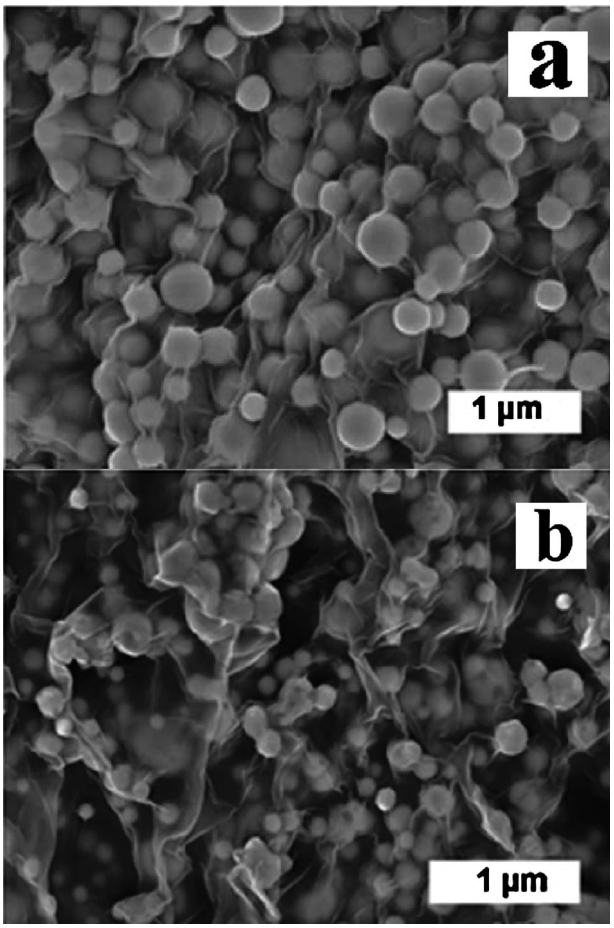

Fig. 5 Typical SEM images of Ag/AgBr/GO (a) and Ag/AgCl/GO (b) composites prepared by a solution mixing method. Reprinted with permission from ref. 103. Copyright 2011, American Chemical Society.

reaction process, GO was reduced to graphene, and simultaneously $ZnFe_2O_4$ nanoparticles were formed on the graphene sheets (as shown in Fig. 6). A graphene–Bi_2WO_6 composite photocatalyst was also prepared by *in situ* hydrothermal reaction in the presence of GO.[95] Furthermore, some solvothermal experiments can result in the semiconductor nanoparticles of special morphology on graphene sheets. For example, Ding *et al.*[114] synthesized graphene-supported

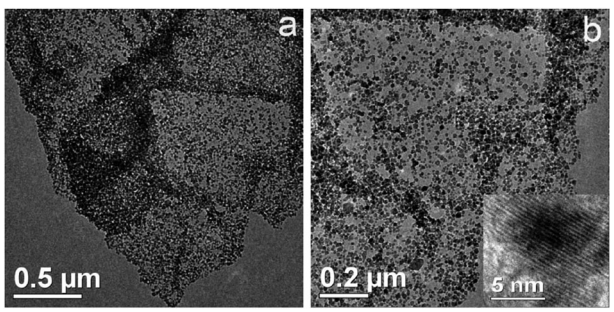

Fig. 6 Typical TEM images of the $ZnFe_2O_4$/graphene composite photocatalyst prepared by an *in situ* hydrothermal method. The inset in (b) shows the high-resolution TEM images of the $ZnFe_2O_4$/graphene composite. Reprinted with permission from ref. 97. Copyright 2011, American Chemical Society.

ultrathin anatase TiO_2 nanosheets with exposed (001) high-energy facets by a simple solvothermal method. In this process, anatase TiO_2 nanosheets directly grew onto the graphene oxide support during the solvothermal growth of TiO_2 nanocrystals, and then GO was reduced to graphene *via* a thermal treatment under N_2/H_2, giving rise to the unique hybrid structure of the graphene–TiO_2 composite. By using a different titanium source, Zhang *et al.*[21] synthesized the graphene–TiO_2 nanocomposite photocatalyst by hydrothermal treatment of graphene oxide sheets and Degussa P25 TiO_2 powder in an ethanol–water solvent. In order to get a uniform mixture of graphene and the semiconductor photocatalyst, Wang *et al.*[115] used a one-step solvothermal method to produce graphene–TiO_2 nanocomposites with well-dispersed particles by controlling the hydrolysis rate of titanium isopropoxide. Very recently, Shen *et al.*[116] found an environmentally friendly route for the preparation of graphene–TiO_2 nanocomposites with a one-step hydrothermal method using glucose as the reducing agent. They claimed that this process is simple, scalable, and feasible because it utilizes only water and glucose.

2.2.4 Other methods. A nonaqueous atomic layer deposition (ALD) approach has been used to fabricate metal oxide–graphene hybrid nanocomposites. For example, Meng *et al.*[83] reported for the first time the preparation of the SnO_2–graphene nanocomposite using $SnCl_4$ and H_2O as the ALD precursors. The SnO_2 nanoparticles/films as well as amorphous/crystalline phases were obtained by adjusting the growth temperature. Moreover, Du *et al.*[88] developed an electrochemical deposition method to prepare the graphene–ZrO_2 composite on a glass carbon electrode.

3. Photocatalytic applications

In recent years, semiconductor-mediated photocatalysis has attracted worldwide attention for its potential in environmental and energy-related applications.[24,35,117–121] However, the rapid recombination rate of photogenerated electron–hole pairs within photocatalytic materials results in its low efficiency, thus limiting its practical applications. Therefore, the suppression of recombination of charge carriers is the key for the enhancement of photocatalytic activity of semiconductor photocatalysts. Besides the conventional doping and adding co-sorbents,[122] carbon–semiconductor hybrid materials became a new class of photocatalysts, which recently has attracted a lot of attention.[123–127] Composites that combine carbon and semiconductor photocatalysts could potentially offer desirable efficiency for separating electron–hole pairs. In this regard, graphene has been examined in combination with a semiconductor photocatalyst, which resulted in improved photocatalytic activity as shown in Table 1. As can be seen from this table the graphene-based semiconductor photocatalysts have been widely used for the degradation of pollutants, photocatalytic hydrogen generation and photocatalytic disinfection, *etc.* In this section the main applications of graphene-based semiconductor photocatalysts are briefly summarized.

3.1 Photocatalytic degradation of pollutants

In recent years, a great deal of effort has been devoted to solving the widespread pollution of effluents from urban and

Table 1 Photocatalytic properties of graphene-semiconductor composite photocatalysts in comparison to the corresponding photocatalysts

Composite photocatalyst	Mass fraction of graphene	Typical parameters of photocatalytic experiments	Photocatalytic activity	Reference photocatalyst; photocatalytic activity	Enhancement factor over the reference photocatalyst	Reference
P25–G	1.0 wt%	Decomposing methylene blue (MB) under UV light	Degradation percentage (DP) of 85%	P25 or P25–CNTs; DP of 25% or 70%, respectively	3.4 or 1.2	21
		Decomposing MB under visible light	DP of 65%	P25 or P25–CNTs; DP of 12% or 52%, respectively	5.4 or 1.25	
P25–G	0.5 wt%	Decomposing benzene (gas phase) under UV light	Conversion of 6.4% in 28 h	P25; conversion of 1.2% in 28 h	5.3	128
	0.2 wt%	Decomposing MB under UV light	DP of 70%	P25; DP of 60%	1.17	
	5.0 wt%		DP of 90%		1.5	
	30 wt%		DP of 58%		0.97	
	0.2 wt%	Decomposing MB under visible light	DP of 40%	P25; DP of 28%	1.4	
	5.0 wt%		DP of 65%		2.3	
	30 wt%		DP of 21%		0.75	
TiO_2–GO	No data	Decomposing MB under UV light	DP of 99% in 15 min	P25; DP of 70% in 15 min	1.4	129
TiO_2–G film	No data	Decomposing 2,4-dichlorophenoxyacetic acid under UV light	Reaction rate: 0.008 min^{-1}	TiO_2 film; reaction rate: 0.002 min^{-1}	4.0	63
TiO_2–G	10 mg	Decomposing MB under sunlight light	DP of 58%	Pure TiO_2 or P25; DP of 25% or 39%, respectively	2.3 or 1.5	130
	30 mg		DP of 75%		3.0 or 1.9	
	50 mg		DP of 72%		2.9 or 1.8	
TiO_2–GO	0.13 wt%	Decomposing methyl orange (MO) under visible light	DP of 26%	P25; DP of 22%	1.18	131
	0.14 wt%		DP of 35%		1.59	
	0.25 wt%		DP of 22%		1.0	
	0.51 wt%		DP of 18%		0.82	
TiO_2–G	0.6 wt%	Decomposing MB under UV light	Reaction rate: 0.071 min^{-1}	TiO_2; reaction rate: 0.045 min^{-1}	1.6	108
TiO_2–G	No data	Decomposing MO under UV light	DP of 85%	Mixture of P25 and graphene; DP of 45%	1.89	132
TiO_2–G/MCM-41	0.05 wt%	Decomposing 2-propanol (gas phase) under UV light	Conversion of 37%	TiO_2/MCM-41; conversion of 26%	1.4	133
	0.15 wt%		Conversion of 45%		1.7	
	0.4 wt%		Conversion of 33%		1.27	
	0.6 wt%		Conversion of 25%		0.96	
TiO_2–G	10 wt%	Decomposing rhodamine B (RhB) under UV light	Reaction rate: 0.20 min^{-1}	Pure TiO_2 or P25; reaction rate: 0.05 min^{-1} or 0.068 min^{-1}, respectively	4.0 or 2.9	134
TiO_2–G	15 wt%	Decomposing RhB under visible light	Reaction rate: 0.0057 min^{-1}	P25; reaction rate: 0.0049 min^{-1}	1.2	81
SnO_2–G	15 wt%		Reaction rate: 0.011 min^{-1}		2.2	
TiO_2–GO	No data	Decomposing MO under UV light	Reaction rate: 0.317 min^{-1}	P25; reaction rate: 0.0426 min^{-1}	7.4	67
		Photo-reductive Cr(VI) under UV light	Conversion rate: 0.0691 min^{-1}	P25; conversion rate: 0.0127 min^{-1}	5.4	
Bi_2WO_6–G	No data	Decomposing RhB under visible light	DP of 90% in 4 min	Bi_2WO_6; DP of 70% in 8 min	> 3.0	95
ZnO–G	0.1 wt%	Decomposing MB under UV light	Reaction rate: 0.047 min^{-1}	ZnO; reaction rate: 0.022 min^{-1}	2.1	75
	0.5 wt%		0.056 min^{-1}		2.5	
	1.0 wt%		0.069 min^{-1}		3.1	
	2.0 wt%		0.098 min^{-1}		4.5	
	3.0 wt%		0.091 min^{-1}		4.1	
	5.0 wt%		0.072 min^{-1}		3.3	
Ag/AgCl/GO	0.6 wt%	Decomposing MO under visible light	DP of 71%	Ag/AgX (X = Br, Cl); DP of 25%	2.8	103
Ag/AgBr/GO			DP of 85%		3.4	
$InNbO_4$–G	No data	Decomposing MB under visible light	Reaction rate: 0.0346 min^{-1}	$InNbO_4$; reaction rate: 0.0185 min^{-1}	1.87	98
		Decomposing 2,4-dichlorophenol under visible light	Reaction rate: 0.0538 min^{-1}	$InNbO_4$; reaction rate: 0.0256 min^{-1}	2.1	
$ZnFe_2O_4$–G	20 wt%	Decomposing MB under visible light	No data	$ZnFe_2O_4$	Enhancement	97
$Sr_2Ta_2O_{7-x}N_x$–G	2.5 wt%	Photocatalytic H_2 evolution under solar light; co-catalyst: Pt; sacrificial reagent: methanol	R_{H_2}: 250 μmol h^{-1}	$Sr_2Ta_2O_{7-x}N_x$; R_{H_2}: 190 μmol h^{-1}	1.3	96
	5.0 wt%		293 μmol h^{-1}		1.5	
	10 wt%		110 μmol h^{-1}		0.58	

Table 1 (*continued*)

Composite photocatalyst	Mass fraction of graphene	Typical parameters of photocatalytic experiments	Photocatalytic activity	Reference photocatalyst; photocatalytic activity	Enhancement factor over the reference photocatalyst	Reference
TiO_2–G	6.5 wt%	Photocatalytic H_2 evolution under UV light; co-catalyst: no; sacrificial reagent: methanol	80 μmol in 5 h	TiO_2; 35 μmol in 5 h	2.3	105
P25–G	5 wt% 10 wt% 20 wt% 30 wt%	Photocatalytic H_2 evolution under UV light; co-catalyst: no; sacrificial reagent: methanol	R_{H_2}: 26 μmol h^{-1} 60 μmol h^{-1} 74 μmol h^{-1} 37 μmol h^{-1}	P25; R_{H_2}: 6.8 μmol h^{-1}	3.8 8.8 10.8 5.4	135
TiO_2–GO	1.0 wt%	Photocatalytic H_2 evolution under UV light; co-catalyst: Pt; sacrificial reagent: methanol	175 mmol in 3 h	TiO_2; 100 mmol in 3 h	1.75	107
$BiVO_4$–G	No data	Photoelectrochemical water splitting	R_{H_2}: 0.75 μmol h^{-1}	$BiVO_4$; R_{H_2}: 0 μmol h^{-1}	~	43
TiO_2–G	25 wt%	Photocatalytic H_2 evolution under UV light; cocatalyst: no; sacrificial reagent: NaS + Na_2SO_3	R_{H_2}: 4.0 μmol h^{-1}	TiO_2; R_{H_2}: 3.4 μmol h^{-1}	1.2	116
TiO_2–G	1.0 wt% 5.0 wt% 10 wt%	Photocatalytic H_2 evolution under UV light; cocatalyst: no; sacrificial reagent: NaS + Na_2SO_3	R_{H_2}: 6.5 μmol h^{-1} 8.6 μmol h^{-1} 4.7 μmol h^{-1}	P25; R_{H_2}: 4.5 μmol h^{-1}	1.4 1.9 1.04	136
CdS–G	0.5 wt% 1.0 wt% 2.5 wt% 5.0 wt% 40 wt%	Photocatalytic H_2 evolution under visible light; cocatalyst: Pt; sacrificial reagent: lactic acid	R_{H_2}: 0.38 μmol h^{-1} 1.12 μmol h^{-1} 0.55 μmol h^{-1} 0.23 μmol h^{-1} 0.02 μmol h^{-1}	CdS; R_{H_2}: 0.23 μmol h^{-1}	1.65 4.87 2.39 1.0 0.087	92
g-C_3N_4/G	0.25 wt% 0.5 wt% 1.0 wt% 2.0 wt% 5.0 wt%	Photocatalytic H_2 evolution under visible light; cocatalyst: Pt; sacrificial reagent: methanol	R_{H_2}: 202 μmol h^{-1} g^{-1} 290 μmol h^{-1} g^{-1} 451 μmol h^{-1} g^{-1} 166 μmol h^{-1} g^{-1} 134 μmol h^{-1} g^{-1}	g-C_3N_4; R_{H_2}: 147 μmol h^{-1} g^{-1}	1.37 1.97 3.07 1.13 0.91	101
CdS/N-doped G	0.5 wt% 1.0 wt% 2.0 wt% 5.0 wt%	Photocatalytic H_2 evolution under visible light; cocatalyst: no; sacrificial reagent: NaS + Na_2SO_3	R_{H_2}: 130 μmol h^{-1} 166 μmol h^{-1} 210 μmol h^{-1} 92 μmol h^{-1}	CdS; R_{H_2}: 40 μmol h^{-1}	3.25 4.15 5.25 2.3	91
CdS/N-doped G	2.0 wt%		R_{H_2}: 210 μmol h^{-1}	CdS/G (2.0 wt%); R_{H_2}: 99 μmol h^{-1}	2.12	
TiO_2–G	No data	Photocatalytic antibacterial activity for killing *E. coli* bacteria under solar light irradiation	Reaction rate: 0.065 min^{-1}	TiO_2; reaction rate: 0.0086 min^{-1}	7.5	112

agricultural industries with biorecalcitrant and organic pollutants. Various catalytic techniques have been applied in environmental protection. Photocatalysis has attracted an increasing attention because of its widespread environmental applications such as air cleanup,[137–139] water disinfection,[140,141] hazardous waste remediation,[142,143] and water purification.[40,144]

Graphene, as a "rising star" material and another allotrope of carbon, has many exceptional properties, such as high electron mobility, theoretically high surface area of 2600 m^2 g^{-1}, and high transparency.[145–149] Therefore, graphene-based semiconductor photocatalysts have been extensively applied to photocatalytic degradation of organic compounds.[150–152] These composites possess high dye adsorption capacity, extended light absorption range, and enhanced charge separation and transportation properties. For example, Zhang *et al.*[21] reported the P25 TiO_2–graphene composite as a high performance photocatalyst. This composite photocatalyst exhibited a significant enhancement of photocatalytic degradation of methylene blue (MB) in water under both UV and visible light irradiation compared to the bare P25. As shown in Fig. 7, MB molecules can be transferred from the solution to the surface of TiO_2 and adsorbed with offset face-to-face orientation *via* π–π conjugation between MB and aromatic regions of graphene, and therefore, adsorption of dyes increases compared to that on the bare P25. Moreover, the extended photoresponding range together with enhanced charge separation and transportation properties resulted in the enhanced photocatalytic activity. In addition, the TiO_2–graphene composite showed higher activity than the P25–carbon nanotubes with the same carbon content because of the giant two-dimensional planar structure of graphene. Such structure can facilitate charge transportation and adsorption of dyes, which are rarely reported in other TiO_2–carbon photocatalysts. However, Zhang and Tang *et al.*[128] found that the TiO_2–graphene composite is in essence the same as other TiO_2–carbon (carbon nanotubes, fullerenes, and activated

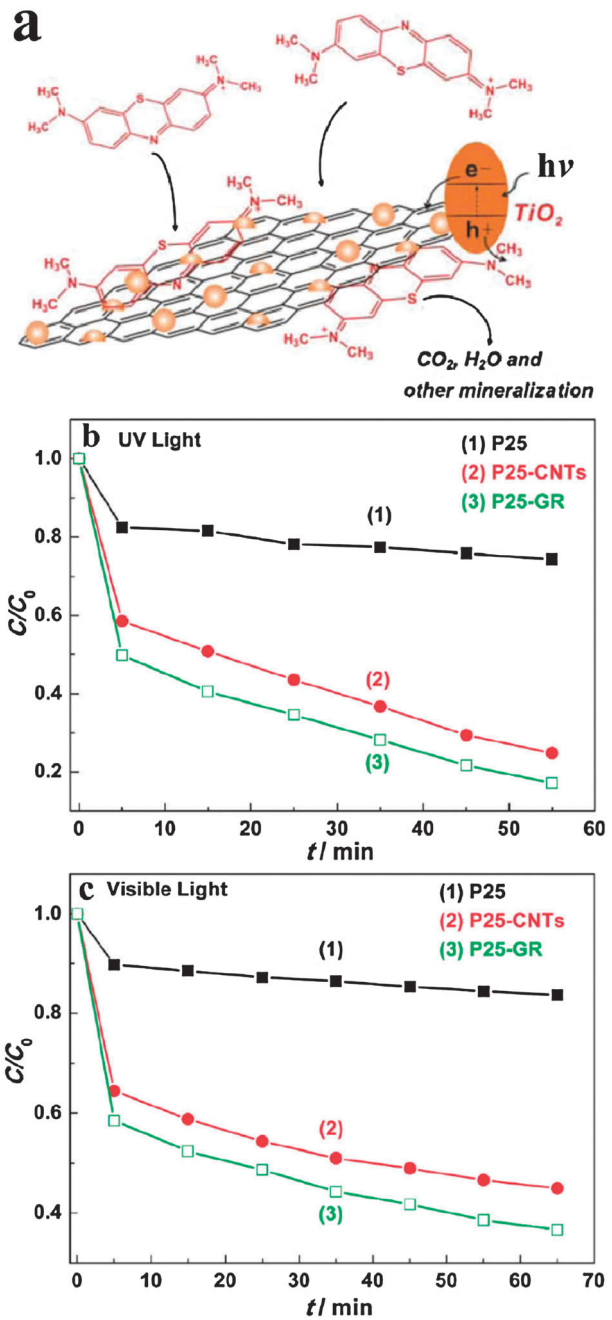

Fig. 7 (a) Schematic structure of the P25–graphene composite illustrating adsorption of methylene blue on graphene sheets, and the role of graphene during the photocatalytic degradation of methylene blue. Comparison of photocatalytic activity in the degradation of methylene blue under (b) UV light and (c) visible light over (1) P25, (2) P25–CNTs, and (3) P25–graphene (P25–GR) photocatalysts. Reprinted with permission from ref. 21. Copyright 2010, American Chemical Society.

carbon) composite materials as regards to the enhancement of photocatalytic activity of TiO_2. They reported that TiO_2–graphene nanocomposite can be used as a photocatalyst under ambient conditions with much higher photocatalytic activity and stability toward the gas-phase degradation of benzene than the bare TiO_2. Furthermore, the effect of the graphene content in the composites on the decomposition of benzene in air and MB in water was also studied (see Fig. 8).

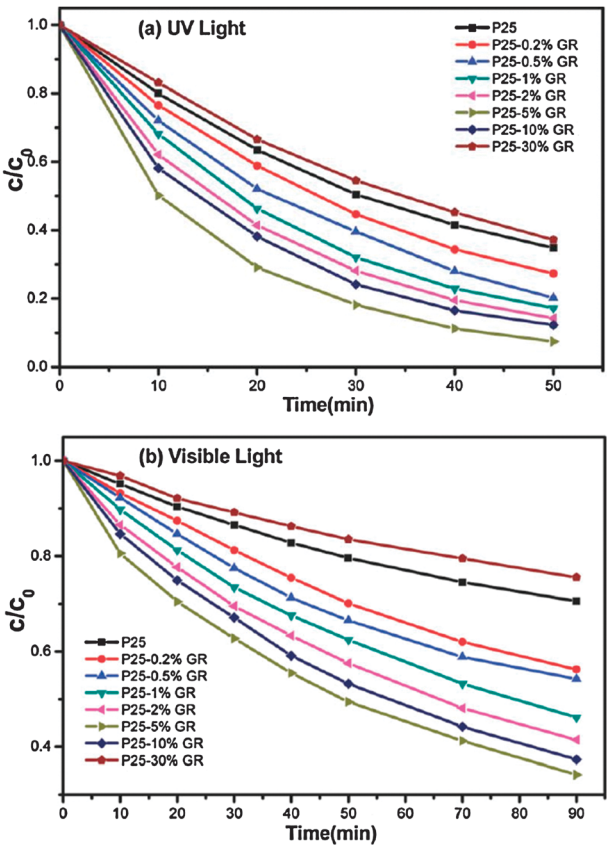

Fig. 8 Comparison of photocatalytic activity for degradation of methylene blue under (a) UV light and (b) visible light over the P25–graphene (P25–GR) nanocomposites with different contents of graphene. Reprinted with permission from ref. 128. Copyright 2010, American Chemical Society.

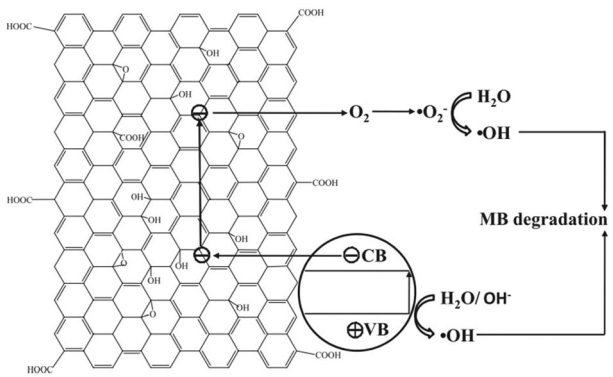

Fig. 9 Illustration of high photocatalytic activity of the TiO_2 nanorods–GO composite for the degradation of methylene blue under UV light irradiation. Reprinted with permission from ref. 129. Copyright 2010, Wiley-VCH.

Liu *et al.*[129] reported the mechanism of anticharge recombination of the TiO_2 nanorods–GO composite for the photocatalytic degradation of MB under UV light irradiation (Fig. 9). They found that the electrons in the GO sheets could react with absorbed O_2 to form $^{\bullet}OH$. Thus, the effective charge transfer can reduce the charge recombination and increase the photocatalytic activity of TiO_2 nanorods.

Furthermore, the TiO_2 nanorods–GO composites showed higher activity than P25–GO composites. This is mainly due to the better contact between GO and TiO_2 nanorods and the more effective charge transfer from TiO_2 nanorods to GO sheets. These results indicate some possibilities for improving the photocatalytic activity of TiO_2–graphene composites by optimizing the morphology of TiO_2 and the distribution of TiO_2 nanoparticles on graphene sheets. For example, Du *et al.*[108] reported the enhanced photocatalytic activity of the hierarchically ordered macro-mesoporous TiO_2–graphene composite films for decomposition of MB in water under UV light irradiation. This hierarchically composite film showed much higher photocatalytic activity than the pure mesoporous TiO_2 film.

Recently, Zhou *et al.*[130] demonstrated that uniform dispersion of anatase TiO_2 nanoparticles with narrow particle size distribution on the surface of graphene sheets assured an enhanced photocatalytic activity in the degradation of MB in water under simulated sunlight irradiation. All the aforementioned results revealed that graphene sheets in the composites can promote charge separation and enhance photocatalytic activity. For the TiO_2–graphene composite, electron–hole pairs are generated within TiO_2 upon excitation under UV light irradiation. These photogenerated electrons tend to transfer to graphene sheets, and then scavenged by dissolved oxygen, facilitating the hole–electron separation.

Meanwhile, the holes can either react with adsorbed water (or surface hydroxyl) to form hydroxyl radicals or directly oxidize various organic compounds. The major reaction steps in this photocatalytic degradation mechanism under UV-light irradiation are summarized by the following eqn (1–5).

$$TiO_2 + h\nu \rightarrow TiO_2\,(e^- + h^+) \quad (1)$$

$$TiO_2\,(e^-) + \text{Graphene} \rightarrow TiO_2 + \text{Graphene}\,(e^-) \quad (2)$$

$$\text{Graphene}\,(e^-) + O_2 \rightarrow \text{Graphene} + O_2^- \quad (3)$$

$$TiO_2\,(h^+) + OH^- \rightarrow TiO_2 + {}^\bullet OH \quad (4)$$

$${}^\bullet OH + \text{Pollutants} \rightarrow \text{Degradation products} \quad (5)$$

It is known that the TiO_2 photocatalyst possesses excellent activity and stability, but requires UV irradiation for effective photocatalysis because of its wide bandgap. It is desirable but challenging to design visible-light responsive photocatalysts. Recently, it was shown that TiO_2–GO and TiO_2–graphene composites can possess visible-light photocatalytic activity due to the presence of carbonate structural fragments bonded with titanium. For example, Chen *et al.*[131] reported the visible-light driven photocatalytic performance of the GO/TiO_2 composites with p/n heterojunction in the degradation of methyl orange (MO). In the aforementioned study, the p-type semiconductor was formed by GO in the GO/TiO_2 composite. Thus, a p/n heterojunction in this composite was observed. Interestingly, this p-type semiconductor could be excited by visible light with wavelengths longer than 510 nm, and acted as a sensitizer and as an electron carrier in the composite, leading to the visible-light responsive photocatalytic activity. This finding might help design a good photosensitizer with graphene oxide in the area of photocatalysis. Very recently, Zhang *et al.*[21] also revealed that the P25 TiO_2–graphene composite showed an enhanced visible-light photocatalytic activity for decomposition of MB in water. This is mainly due to the fact that graphene in this composite can enhance the light absorption range, promote charge separation and increase adsorption of pollutants.

Apart from TiO_2–graphene composites, composites of graphene and other semiconductor photocatalysts such as SnO_2–graphene,[81] ZnO–graphene,[48] Bi_2WO_6–graphene,[95] Ag/AgCl/GO,[102,103] Ag/AgBr/GO,[103] $ZnFe_2O_4$–graphene,[97] $InNbO_4$–graphene[98] and γ-Bi_2MoO_6/graphene[99] have been reported as efficient photocatalysts for decomposition of pollutants in water. For instance, Zhang *et al.*[81] evaluated the visible-light photocatalytic activity of SnO_2–graphene and TiO_2–graphene composites for degradation of self-photosensitized rhodamine B (RhB) in water, and found that both these composites exhibited excellent photocatalytic performance. This could be attributed to the good electrical conductivity and effective charge separation because of the presence of graphene in these composites. Surprisingly, the SnO_2–graphene composite system showed better photocatalytic activity than TiO_2–graphene. This is mainly due to the fact that the electron transfer from RhB* to SnO_2 is thermodynamically more favorable because of the large potential difference between the RhB* and SnO_2. Moreover, Xu and co-workers[75] reported the graphene hybridized ZnO composite as an efficient photocatalyst. This composite also showed enhanced photocatalytic activity for the degradation of MB aqueous solution under UV irradiation. Recently, the Bi_2WO_6–graphene composite photocatalysts were studied by Gao and co-workers[95] for the photocatalytic degradation of RhB solution under visible light irradiation. As shown in Fig. 10, electronic interactions and charge equilibration between graphene and Bi_2WO_6 led to the shift in the Fermi level and decreased the conduction band potential of Bi_2WO_6. Thus, the negative shift in the Fermi level of G-BWO and the high migration efficiency of photoinduced electrons can suppress the charge recombination effectively, resulting in the enhanced photocatalytic activity.

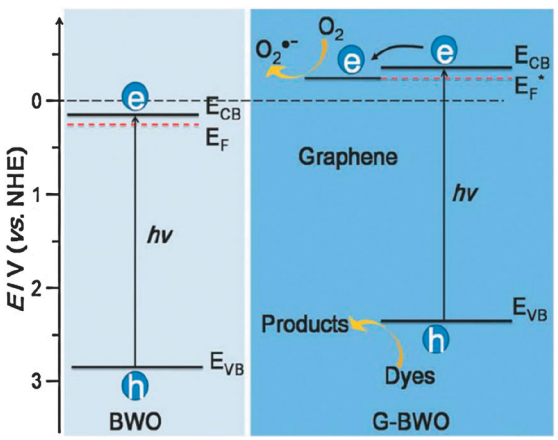

Fig. 10 Energy-level diagram and photocatalysis scheme for pure Bi_2WO_6 and Bi_2WO_6–graphene composites. Reprinted with permission from ref. 95. Royal Society of Chemistry.

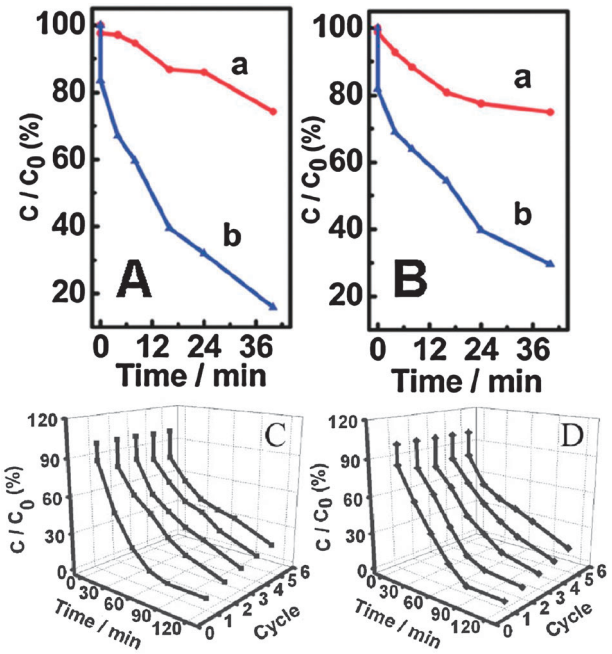

Fig. 11 Comparison of photocatalytic activity for the degradation of methylene orange under visible light irradiation over the system (A) of Ag/AgBr (a) and Ag/AgBr/GO composite (b), and the system (B) of Ag/AgCl (a) and Ag/AgCl/GO composite (b). The cycling curves for degradation of methylene orange over Ag/AgBr/GO (C) and Ag/AgCl/GO (D) composites. Reprinted with permission from ref. 103. Copyright 2011, American Chemical Society.

Very recently, Zhu *et al.*[103] for the first time reported GO enwrapped Ag/AgX (X = Br, Cl) composites as highly efficient visible-light plasmonic photocatalysts. These photocatalysts displayed an enhanced visible-light photocatalytic activity for photocatalytic degradation of MO in water and high stability as shown in Fig. 11. This observed enhancement was due to the hybridization of Ag/AgX with GO, which improved adsorption affinity of Ag/AgX/GO towards MO molecules. Also, the smaller size of the Ag/AgX nanoparticles in Ag/AgX/GO, the facilitated charge transfer, and the suppressed recombination of electron–hole pairs in the Ag/AgX/GO composite contributed to this enhancement. In another system, graphene sheets were introduced into a visible-light driven $ZnFe_2O_4$ photocatalyst for photocatalytic decomposition of MB in water.[97] In comparison to pure $ZnFe_2O_4$, $ZnFe_2O_4$–graphene showed a significant enhancement in the photocatalytic activity due to the efficient separation of photogenerated carriers in the $ZnFe_2O_4$ and graphene coupling system.

3.2 Photocatalytic hydrogen generation

Hydrogen energy is regarded as an ultimate clean fuel in the future because of its high-energy capacity, environmental friendliness, and recycling possibility.[42,153,154] Photocatalytic water splitting into hydrogen and oxygen using semiconductor photocatalysts has been considered as a promising and attractive approach to produce hydrogen energy. A variety of semiconductor photocatalysts have been reported to catalyze the evolution of hydrogen from water. However, the practical applications of this strategy are limited due to the rapid recombination of photogenerated electrons and holes within photocatalysts. Considering the superior electron mobility and high specific surface area, graphene can be used as an efficient electron acceptor to enhance the photoinduced charge transfer and to inhibit the backward reaction by separating the evolution sites of hydrogen and oxygen (see Fig. 12) for improved photocatalytic H_2-production activity.[19]

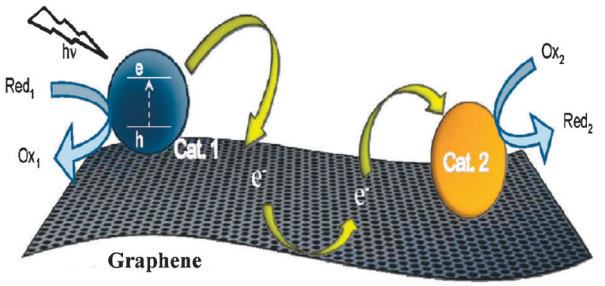

Fig. 12 Schematic illustration of selective catalysis at different sites on graphene used as a conducting support. Reprinted with permission from ref. 19. Copyright 2010, American Chemical Society.

Using the graphene/TiO_2 composites with different loading contents of graphene, Cui and co-workers[136,155,156] studied their water splitting performance using Na_2S and Na_2SO_3 as sacrificial agents under Xe lamp irradiation. The optimal graphene content was found to be 5.0 wt%, giving a H_2-production rate of 8.6 μmol h^{-1}, which exceeded the rate on pure P25 TiO_2 by more than 2 times.[136] The enhanced photocatalytic H_2-production activity was due to the deposition of TiO_2 nanoparticles on graphene sheets, which acted as electron acceptors to efficiently separate the photogenerated charge carriers. Very recently, Fan *et al.*[135] systematically studied the efficiency of H_2 evolution for the P25–graphene composite prepared by UV-assisted photocatalytic reduction, hydrazine reduction, and a hydrothermal method. As shown in Fig. 13, all of these

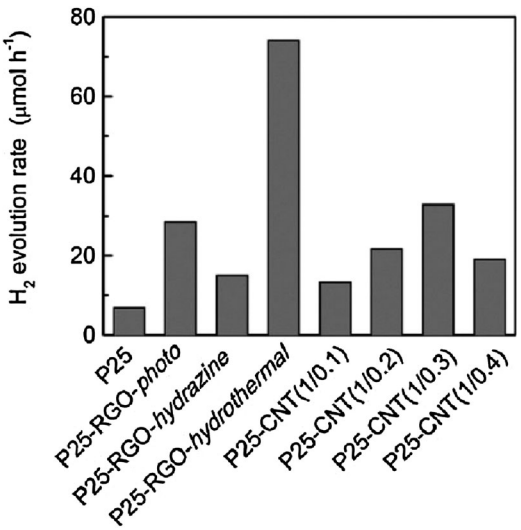

Fig. 13 Comparison of photocatalytic activity of P25, P25–graphene (P25–RGO) composites (mass ratio of P25/RGO = 1/0.2) prepared by different methods, and P25–CNT composites with different mass ratios of P25/CNT for the evolution of H_2 from methanol aqueous solution. Reprinted with permission from ref. 135. Copyright 2011, American Chemical Society.

composites exhibited better photocatalytic performance for H_2 evolution from methanol aqueous solution than P25 alone, and the P25–graphene composite prepared by the hydrothermal method possessed the best performance. The ratio of P25/graphene in the composite also significantly influenced the photocatalytic performance, and the optimum mass ratio has been found to be 1/0.2, giving a H_2-production rate of 74 μmol h^{-1}. This value exceeds that of pure P25 by more than 10 times. Moreover, this composite was stable and recyclable, and even it could photocatalyze the evolution of H_2 from pure water without co-catalysts. In order to further explore the possible application of TiO_2 based-graphene composites in hydrogen production, Choi and co-workers[107] showed that the graphite oxide on titania nanoparticles is an efficient auxiliary co-catalyst for the photocatalytic hydrogen production. They found that a hybrid of GO/TiO_2 showed an enhanced activity for both photocurrent generation and hydrogen production than bare TiO_2 under UV light irradiation. In particular, the photocatalytic production of hydrogen was markedly enhanced in the co-presence of GO sheets along with Pt on the surface of TiO_2, which indicated that the cheap and abundant carbon material can be a good candidate for finding an electron attracting reservoir and an auxiliary co-catalyst for photocatalytic hydrogen production.

Even though the photocatalytic hydrogen production of TiO_2 nanoparticles has been extensively investigated, the hydrogen evolution rate of such photocatalysts is generally still much lower than that of the state-of-the-art benchmarking photocatalysts such as lanthanum-doped $NaTaO_3$, nitrogen-doped $Sr_2Ta_2O_7$, and Pt–CdS. A further enhancement of the water splitting performance of these state-of-the-art photocatalysts was proposed by introduction of graphene. For example, Mukherji *et al.*[96] reported nitrogen doped $Sr_2Ta_2O_7$ coupled with graphene sheets as photocatalysts for increased photocatalytic hydrogen production under solar irradiation. By using graphene as a support for the Pt co-catalyst, the composite containing graphene–Pt and $Sr_2Ta_2O_{7-x}N$ showed a hydrogen evolution rate of 293 μmol h^{-1} with a quantum efficiency (QE) of 6.45% under 280–550 nm light irradiation. However, the corresponding rates for pure $Sr_2Ta_2O_7$ with the Pt co-catalyst and $Sr_2Ta_2O_{7-x}N$–Pt without graphene were 106 μmol h^{-1} with a QE of 2.33% and 194 μmol h^{-1} with a QE of 4.26% under the same measurement conditions, respectively. Thus, nitrogen doping and usage of graphene as a conductive electron transport "highway" resulted in the improvement of the hydrogen production efficiency in comparison to that of the pristine $Sr_2Ta_2O_7$ photocatalyst. Similarly, Jia *et al.*[91] studied the photocatalytic H_2-production activity of a series of N-doped graphene/CdS nanocomposites from aqueous solutions containing Na_2S and Na_2SO_3 as sacrificial agents under visible-light irradiation. As shown in Fig. 14, the hydrogen evolution rate of CdS was significantly enhanced by loading N-doped graphene. The optimal loading content of N-doped graphene was found to be 2.0 wt%, giving a H_2-production rate of 210 μmol h^{-1}, exceeding that on pure CdS (40 μmol h^{-1}) by more than 5 times. The enhanced mechanism is because the potential of graphene/graphene$^-$ is lower than the conduction band of CdS, meanwhile higher than the reduction potential of H^+, which favors the electron transfer from the conduction band

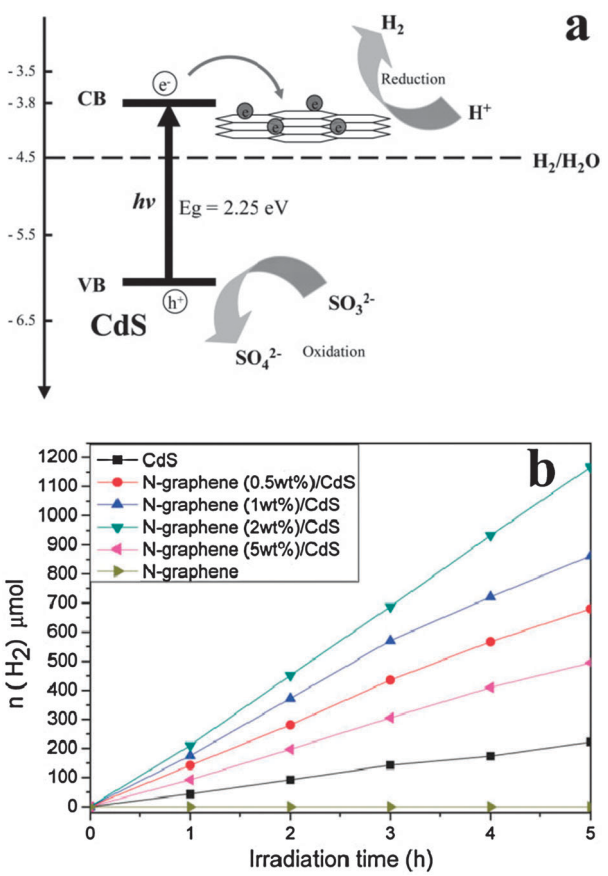

Fig. 14 (a) Energy-level diagram of N-graphene/CdS nanocomposites in relation to the redox potentials for the water spitting process in Na_2S/Na_2SO_3 aqueous solution under visible light irradiation. (b) Comparison of the photocatalytic activity of N-graphene/CdS composites with different contents of N-graphene for the photocatalytic H_2 production from Na_2S/Na_2SO_3 aqueous solution under visible-light irradiation. Reprinted with permission from ref. 91. Copyright 2011, American Chemical Society.

of CdS to graphene sheets and the reduction of H^+, thus enhancing photocatalytic H_2-production activity.

Also, a metal-free polymeric photocatalyst, graphitic carbon nitride (g-C_3N_4), showed a good photocatalytic performance for hydrogen or oxygen production *via* water splitting under visible-light irradiation.[157] Combining g-C_3N_4 with graphene sheets gave rise to an increased conductivity and catalytic performance. The resulting graphene/g-C_3N_4 composites showed a H_2-evolution rate 3.0 times higher than pure g-C_3N_4 under visible-light irradiation due to the efficient charge carrier separation on the photocatalyst as shown in Fig. 15.[101] Similarly, Ng *et al.*[43] reported that the reduced GO on a visible-light $BiVO_4$ photocatalyst showed an enhanced photoelectrochemical water splitting. Compared with pure $BiVO_4$, the photoelectrochemical water splitting reaction rate based on the graphene/$BiVO_4$ composite showed nearly 10-fold enhancement at a 0.8 V bias under visible-light illumination. This significant improvement was attributed to the introduction of graphene sheets, which facilitated the electron transport between illuminated $BiVO_4$ and the electrode, leading to a minimized recombination of

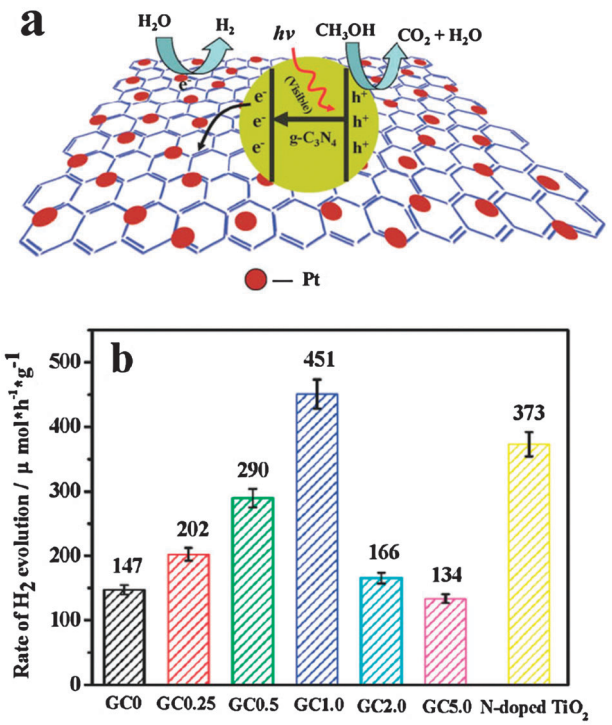

Fig. 15 (a) Proposed mechanism for the enhanced electron transfer over the graphene/g-C_3N_4 composites for the water spitting process in methanol aqueous solution under visible-light irradiation. (b) Comparison of the photocatalytic activity of the graphene/g-C_3N_4 composites with different contents of graphene for the evolution of H_2 from methanol aqueous solution under visible-light irradiation. Reprinted with permission from ref. 101. Copyright 2011, American Chemical Society.

photoelectrons and holes. Moreover, the incident photon-to-current-conversion efficiency (IPCE) of the graphene/$BiVO_4$ composite was measured to be 4.2%, which is one order of magnitude greater than that of pure $BiVO_4$ (0.3% at 400 nm).

Interestingly, graphite oxide itself with an appropriately oxidized level can also serve as a photocatalyst for hydrogen production. Teng and co-workers[158] reported that a graphite oxide semiconductor photocatalyst with a band gap of 2.4–4.3 eV can steadily produce H_2 from an aqueous methanol solution or pure water, even in the absence of Pt as the co-catalyst under visible light irradiation (Fig. 16). Usually, the band gap energy of graphite oxide depends on the number of oxygenated sites, and can be modulated by functionalization or cutting them into nanoribbons. When the conduction band

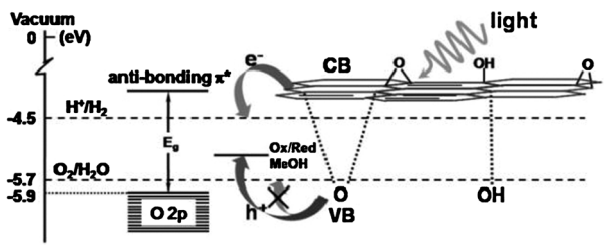

Fig. 16 Energy-level diagram of semiconducting graphene oxide illustrating the promising photocatalyst for water spitting. Reprinted with permission from ref. 158. Copyright 2010, Wiley-VCH.

edge of graphite oxide, which is mainly formed by the anti-bonding π* orbital, has a higher energy level than that needed for H_2 generation, it can lead to electron injection into the solution phase for H_2 generation.

3.3 Photocatalytic disinfection

TiO_2-mediated disinfection has been considered as a promising process compared to the common disinfection methods such as chlorination and UV disinfection for its strong oxidizing power, nontoxicity, and long-term photostability, also requiring little or no maintenance.[140] Since the use of graphene may enhance the photocatalytic properties of TiO_2 under UV and visible-light irradiation, graphene–TiO_2 composites may potentially be used to enhance the bactericidal activity. For example, Akhavan and Ghaderi[112] found that the graphene/TiO_2 composite thin films were able to destroy more than 99.9% of *E. coli* bacteria in an aqueous solution under solar light irradiation. Such antibacterial activity was significantly improved as compared to the pure TiO_2 thin film by a factor of about 7.5. Furthermore, the graphene platelets were chemically stable after photoinactivation of the bacteria.

4. Conclusion and perspectives

In summary, functional graphene can be introduced into various semiconductor photocatalysts to form graphene-based semiconductor composites. The incorporation of graphene into these composites can improve them with unique properties of graphene and possibly induce new properties, such as high dye adsorption capacity, extended light absorption range, and enhanced charge separation and transportation properties, which enhance the overall photocatalytic performance. A variety of methods such as *in situ* growth, solution mixing, hydrothermal and/or solvothermal strategies have been developed for fabricating the graphene-based semiconductor photocatalysts. These composite photocatalysts have been widely used for the degradation of pollutants, photocatalytic hydrogen generation and photocatalytic disinfection.

Graphene-based semiconductor photocatalysts have attracted extensive attention for their potential in environmental and energy-related applications. Although considerable progress has been achieved, the studies in this field are at the primary stage and further developments are required. First, as an essential component of the composites, the synthesis of graphene is not yet matured and the quality-control issues need to be addressed. New synthesis methods have to be developed for preparing high-quality graphene or graphene oxide sheets with high purity, tunable sizes of layers, compositions and defects. Second, the performance of graphene-based semiconductor composites is limited by the quantity of these composites and their microstructures. Therefore, a more careful design of the functional composites is required to obtain higher quality, more uniform morphology on the nanoscale and better photocatalytic properties. Third, the rapid development of material science and technique in the past few years has resulted in the creation of various advanced photocatalytic materials. Interesting properties may be explored by combining these novel photocatalysts with graphene or graphene oxide sheets. Finally, the mechanisms of photocatalytic enhancement by the graphene-based

semiconductor composite systems are partly unclear. For example, whether the photocatalytic activity of TiO_2–graphene composites is truly different from other TiO_2–C (activated carbon, fullerenes, or carbon nanotubes) composite materials. Furthermore, the explanation of photocatalytic activity by the graphene content in the composites is still controversial. Therefore, more studies are needed to improve the general understanding of the enhancement mechanism of photocatalysts by graphene. Nevertheless, graphene-based semiconductor composite photocatalysts are expected to be developed as robust materials to address various environmental and energy-related issues.

Acknowledgements

This work was partially supported by the National Basic Research Program of China (2007CB613302 and 2009CB939704), National Natural Science Foundation of China (20877061 and 51072154), Natural Science Foundation of Hubei Province (2010CDA078), Fundamental Research Funds for the Central Universities (2010-YB-01) and Self-determined and Innovative Research Funds of SKLWUT.

Notes and references

1 K. S. Novoselov, A. K. Geim, S. V. Morozov, D. Jiang, Y. Zhang, S. V. Dubonos, I. V. Grigorieva and A. A. Firsov, *Science*, 2004, **306**, 666.
2 A. K. Geim and K. S. Novoselov, *Nat. Mater.*, 2007, **6**, 183.
3 M. J. Allen, V. C. Tung and R. B. Kaner, *Chem. Rev.*, 2010, **110**, 132.
4 A. K. Geim, *Science*, 2009, **324**, 1530.
5 X. S. Li, W. W. Cai, J. H. An, S. Kim, J. Nah, D. X. Yang, R. Piner, A. Velamakanni, I. Jung, E. Tutuc, S. K. Banerjee, L. Colombo and R. S. Ruoff, *Science*, 2009, **324**, 1312.
6 K. S. Kim, Y. Zhao, H. Jang, S. Y. Lee, J. M. Kim, K. S. Kim, J. H. Ahn, P. Kim, J. Y. Choi and B. H. Hong, *Nature*, 2009, **457**, 706.
7 C. N. R. Rao, A. K. Sood, K. S. Subrahmanyam and A. Govindaraj, *Angew. Chem., Int. Ed.*, 2009, **48**, 7752.
8 Y. Q. Sun, Q. O. Wu and G. Q. Shi, *Energy Environ. Sci.*, 2011, **4**, 1113.
9 H. Bai, C. Li and G. Q. Shi, *Adv. Mater.*, 2011, **23**, 1089.
10 S. Park and R. S. Ruoff, *Nat. Nanotechnol.*, 2009, **4**, 217.
11 S. Stankovich, D. A. Dikin, G. H. B. Dommett, K. M. Kohlhaas, E. J. Zimney, E. A. Stach, R. D. Piner, S. T. Nguyen and R. S. Ruoff, *Nature*, 2006, **442**, 282.
12 K. Wang, J. Ruan, H. Song, J. Zhang, Y. Wo, S. Guo and D. Cui, *Nanoscale Res. Lett.*, 2011, **6**, 8.
13 Q. Wang, X. Guo, L. Cai, Y. Cao, L. Gan, S. Liu, Z. Wang, H. Zhang and L. Li, *Chem. Sci.*, 2011, DOI: 10.1039/c1sc00344e.
14 S. Park, N. Mohanty, J. W. Suk, A. Nagaraja, J. An, R. D. Piner, W. Cai, D. R. Dreyer, V. Berry and R. S. Ruoff, *Adv. Mater.*, 2010, **22**, 1736.
15 W. B. Cai and X. Y. Chen, *Small*, 2007, **3**, 1840.
16 O. Akhavan, E. Ghaderi and A. Esfandiar, *J. Phys. Chem. B*, 2011, **115**, 6279.
17 (*a*) A. J. Du, Y. H. Ng, N. J. Bell, Z. H. Zhu, R. Amal and S. C. Smith, *J. Phys. Chem. Lett.*, 2011, **2**, 894; (*b*) J. J. Guo, S. M. Zhu, Z. X. Chen, Y. Li, Z. Y. Yu, Q. L. Liu, J. B. Li, C. L. Feng and D. Zhang, *Ultrason. Sonochem.*, 2011, **18**, 1082; (*c*) J. H. Liu, Z. C. Wang, L. W. Liu and W. Chen, *Phys. Chem. Chem. Phys.*, 2011, **13**, 13216; (*d*) Y. H. Ng, A. Iwase, N. J. Bell, A. Kudo and R. Amal, *Catal. Today*, 2011, **164**, 353.
18 (*a*) R. Leary and A. Westwood, *Carbon*, 2011, **49**, 741; (*b*) Q. J. Xiang, J. G. Yu and M. Jaroniec, *Nanoscale*, 2011, DOI: 10.1039/c1nr10610d; (*c*) B. Jiang, C. Tian, W. Zhou, J. Wang, Y. Xie, Q. Pan, Z. Ren, Y. Dong, D. Fu, J. Han and H. Fu, *Chem.–Eur. J.*, 2011, **17**, 8379; (*d*) Y. T. Liang, B. K. Vijayan, K. A. Gray and M. C. Hersam, *Nano Lett.*, 2011, **11**, 2865.
19 I. V. Lightcap, T. H. Kosel and P. V. Kamat, *Nano Lett.*, 2010, **10**, 577.
20 G. Williams, B. Seger and P. V. Kamat, *ACS Nano*, 2008, **2**, 1487.
21 H. Zhang, X. J. Lv, Y. M. Li, Y. Wang and J. H. Li, *ACS Nano*, 2010, **4**, 380.
22 S. Wang, B. M. Goh, K. K. Manga, Q. L. Bao, P. Yang and K. P. Loh, *ACS Nano*, 2010, **4**, 6180.
23 A. Fujishima and K. Honda, *Nature*, 1972, **238**, 37.
24 M. R. Hoffmann, S. T. Martin, W. Choi and D. W. Bahnemann, *Chem. Rev.*, 1995, **95**, 69.
25 A. Kudo and Y. Miseki, *Chem. Soc. Rev.*, 2009, **38**, 253.
26 X. B. Chen, S. H. Shen, L. J. Guo and S. S. Mao, *Chem. Rev.*, 2010, **110**, 6503.
27 J. C. Yu, J. G. Yu, W. K. Ho, Z. T. Jiang and L. Z. Zhang, *Chem. Mater.*, 2002, **14**, 3808.
28 Y. W. Cheng, R. C. Y. Chan and P. K. Wong, *Water Res.*, 2007, **41**, 842.
29 P. Panagiotopoulou, A. Christodoulakis, D. I. Kondarides and S. Boghosian, *J. Catal.*, 2006, **240**, 114.
30 H. G. Yang, C. H. Sun, S. Z. Qiao, J. Zou, G. Liu, S. C. Smith, H. M. Cheng and G. Q. Lu, *Nature*, 2008, **453**, 638.
31 S. I. In, Y. D. Hou, B. L. Abrams, P. C. K. Vesborg and I. Chorkendorff, *J. Electrochem. Soc.*, 2010, **157**, E69.
32 S. W. Liu, J. G. Yu and M. Jaroniec, *J. Am. Chem. Soc.*, 2010, **132**, 11914.
33 (*a*) Q. J. Xiang, J. G. Yu and M. Jaroniec, *Chem. Commun.*, 2011, **47**, 4532; (*b*) Q. J. Xiang and J. G. Yu, *Chin. J. Catal.*, 2011, **32**, 525; (*c*) J. G. Yu and J. Zhang, *Dalton Trans.*, 2010, **39**, 5860.
34 M. Ksibi, S. Rossignol, J. M. Tatibouet and C. Trapalis, *Mater. Lett.*, 2008, **62**, 4204.
35 J. H. Park, S. Kim and A. J. Bard, *Nano Lett.*, 2006, **6**, 24.
36 (*a*) Q. J. Xiang, J. G. Yu and M. Jaroniec, *Phys. Chem. Chem. Phys.*, 2011, **13**, 4853; (*b*) Q. J. Xiang, J. G. Yu, W. G. Wang and M. Jaroniec, *Chem. Commun.*, 2011, **47**, 6906; (*c*) S. W. Liu, C. Li, J. G. Yu and Q. J. Xiang, *CrystEngComm*, 2011, **13**, 2533; (*d*) S. W. Liu, J. G. Yu and W. G. Wang, *Phys. Chem. Chem. Phys.*, 2010, **12**, 12308.
37 J. G. Yu, Q. J. Xiang and M. H. Zhou, *Appl. Catal., B*, 2009, **90**, 595.
38 J. G. Yu, J. F. Xiong, B. Cheng and S. W. Liu, *Appl. Catal., B*, 2005, **60**, 211.
39 J. G. Yu, L. F. Qi and M. Jaroniec, *J. Phys. Chem. C*, 2010, **114**, 13118.
40 Q. J. Xiang, J. G. Yu, B. Cheng and H. C. Ong, *Chem.–Asian. J.*, 2010, **5**, 1466.
41 K. Woan, G. Pyrgiotakis and W. Sigmund, *Adv. Mater.*, 2009, **21**, 2233.
42 J. G. Yu, J. Zhang and M. Jaroniec, *Green Chem.*, 2010, **12**, 1611.
43 Y. H. Ng, A. Iwase, A. Kudo and R. Amal, *J. Phys. Chem. Lett.*, 2010, **1**, 2607.
44 Y. H. Ng, A. Iwase, N. J. Bell, A. Kudo and R. Amal, *Catal. Today*, 2011, **164**, 353.
45 H. T. Hu, X. B. Wang, F. M. Liu, J. C. Wang and C. H. Xu, *Synth. Met.*, 2011, **161**, 404.
46 T. N. Lambert, C. A. Chavez, N. S. Bell, C. M. Washburn, D. R. Wheeler and M. T. Brumbach, *Nanoscale*, 2011, **3**, 188.
47 Y. P. Zhang and C. X. Pan, *J. Mater. Sci.*, 2011, **46**, 2622.
48 B. J. Li and H. Q. Cao, *J. Mater. Chem.*, 2011, **21**, 3346.
49 O. V. Prezhdo, P. V. Kamat and G. C. Schatz, *J. Phys. Chem. C*, 2011, **115**, 3195.
50 P. V. Kamat, *J. Phys. Chem. Lett.*, 2011, **2**, 242.
51 K. V. Emtsev, A. Bostwick, K. Horn, J. Jobst, G. L. Kellogg, L. Ley, J. L. McChesney, T. Ohta, S. A. Reshanov, J. Rohrl, E. Rotenberg, A. K. Schmid, D. Waldmann, H. B. Weber and T. Seyller, *Nat. Mater.*, 2009, **8**, 203.
52 Z. Y. Juang, C. Y. Wu, A. Y. Lu, C. Y. Su, K. C. Leou, F. R. Chen and C. H. Tsai, *Carbon*, 2010, **48**, 3169.
53 D. C. Wei, Y. Q. Liu, Y. Wang, H. L. Zhang, L. P. Huang and G. Yu, *Nano Lett.*, 2009, **9**, 1752.
54 S. Park, J. H. An, I. W. Jung, R. D. Piner, S. J. An, X. S. Li, A. Velamakanni and R. S. Ruoff, *Nano Lett.*, 2009, **9**, 1593.
55 D. Li, M. B. Muller, S. Gilje, R. B. Kaner and G. G. Wallace, *Nat. Nanotechnol.*, 2008, **3**, 101.

56 M. J. McAllister, J. L. Li, D. H. Adamson, H. C. Schniepp, A. A. Abdala, J. Liu, M. Herrera-Alonso, D.L. Milius, R. Car, R. K. Prud'homme and I. A. Aksay, *Chem. Mater*., 2007, **19**, 4396.
57 V. C. Tung, M. J. Allen, Y. Yang and R. B. Kaner, *Nat. Nanotechnol*., 2009, **4**, 25.
58 W. S. Hummers and R. E. Offeman, *J. Am. Chem. Soc*., 1958, **80**, 1339.
59 H. C. Schniepp, J. L. Li, M. J. McAllister, H. Sai, M. Herrera-Alonso, D. H. Adamson, R. K. Prud'homme, R. Car, D. A. Saville and I. A. Aksay, *J. Phys. Chem. B*, 2006, **110**, 8535.
60 X. F. Gao, J. Jang and S. Nagase, *J. Phys. Chem. C*, 2010, **114**, 832.
61 G. K. Ramesha and S. Sampath, *J. Phys. Chem. C*, 2009, **113**, 7985.
62 V. Abdelsayed, S. Moussa, H. M. Hassan, H. S. Aluri, M. M. Collinson and M. S. El-Shall, *J. Phys. Chem. Lett*., 2010, **1**, 2804.
63 Y. H. Ng, I. V. Lightcap, K. Goodwin, M. Matsumura and P. V. Kamat, *J. Phys. Chem. Lett*., 2010, **1**, 2222.
64 K. Vinodgopal, B. Neppolian, I. V. Lightcap, F. Grieser, M. Ashokkumar and P. V. Kamat, *J. Phys. Chem. Lett*., 2010, **1**, 1987.
65 K. Jasuja, J. Linn, S. Melton and V. Berry, *J. Phys. Chem. Lett*., 2010, **1**, 1853.
66 L. M. Zhang, S. O. Diao, Y. F. Nie, K. Yan, N. Liu, B. Y. Dai, Q. Xie, A. Reina, J. Kong and Z. F. Liu, *J. Am. Chem. Soc*., 2011, **133**, 2706.
67 G. D. Jiang, Z. F. Lin, C. Chen, L. H. Zhu, Q. Chang, N. Wang, W. Wei and H. Q. Tang, *Carbon*, 2011, **49**, 2693.
68 K. K. Manga, Y. Zhou, Y. L. Yan and K. P. Loh, *Adv. Funct. Mater*., 2009, **19**, 3638.
69 O. Akhavan, M. Abdolahad, A. Esfandiar and M. Mohatashamifar, *J. Phys. Chem. C*, 2010, **114**, 12955.
70 Y. Fan, K. J. Huang, D. J. Niu, C. P. Yang and Q. S. Jing, *Electrochim. Acta*, 2011, **56**, 4685.
71 F. Zou, Y. A. Yu, N. Cao, L. Z. Wu and J. F. Zhi, *Scr. Mater*., 2011, **64**, 621.
72 Y. C. Qiu, K. Y. Yan, S. H. Yang, L. M. Jin, H. Deng and W. S. Li, *ACS Nano*, 2010, **4**, 6515.
73 N. L. Yang, J. Zhai, D. Wang, Y. S. Chen and L. Jiang, *ACS Nano*, 2010, **4**, 887.
74 Y. B. Tang, C. S. Lee, J. Xu, Z. T. Liu, Z. H. Chen, Z. B. He, Y. L. Cao, G. D. Yuan, H. S. Song, L. M. Chen, L. B. Luo, H. M. Cheng, W. J. Zhang, I. Bello and S. T. Lee, *ACS Nano*, 2010, **4**, 3482.
75 T. G. Xu, L. W. Zhang, H. Y. Cheng and Y. F. Zhu, *Appl. Catal., B*, 2011, **101**, 382.
76 O. Akhavan, *Carbon*, 2011, **49**, 11.
77 O. Akhavan, *ACS Nano*, 2010, **4**, 4174.
78 G. Williams and P. V. Kamat, *Langmuir*, 2009, **25**, 13869.
79 T. Lu, L. K. Pan, H. B. Li, G. A. Zhu, T. A. Lv, X. J. Liu, Z. Sun, T. Chen and D. H. C. Chua, *J. Alloys Compd*., 2011, **509**, 5488.
80 J. M. Lee, Y. B. Pyun, J. Yi, J. W. Choung and W. I. Park, *J. Phys. Chem. C*, 2009, **113**, 19134.
81 J. T. Zhang, Z. G. Xiong and X. S. Zhao, *J. Mater. Chem*., 2011, **21**, 3634.
82 E. Yoo, J. Kim, E. Hosono, H. Zhou, T. Kudo and I. Honma, *Nano Lett*., 2008, **8**, 2277.
83 X. B. Meng, D. S. Geng, J. A. Liu, M. N. Banis, Y. Zhang, R. Y. Li and X. L. Sun, *J. Phys. Chem. C*, 2010, **114**, 18330.
84 C. Xu, X. Wang and J. W. Zhu, *J. Phys. Chem. C*, 2008, **112**, 19841.
85 K. Morishige and T. Hamada, *Langmuir*, 2005, **21**, 6277.
86 D. H. Wang, R. Kou, D. Choi, Z. G. Yang, Z. M. Nie, J. Li, L. V. Saraf, D. H. Hu, J. G. Zhang, G. L. Graff, J. Liu, M. A. Pope and I. A. Aksay, *ACS Nano*, 2010, **4**, 1587.
87 J. Yan, Z. J. Fan, T. Wei, W. Z. Qian, M. L. Zhang and F. Wei, *Carbon*, 2010, **48**, 3825.
88 D. Du, J. Liu, X. Y. Zhang, X. L. Cui and Y. H. Lin, *J. Mater. Chem*., 2011, **21**, 8032.
89 C. Nethravathi, T. Nisha, N. Ravishankar, C. Shivakumara and M. Rajamathi, *Carbon*, 2009, **47**, 2054.
90 A. N. Cao, Z. Liu, S. S. Chu, M. H. Wu, Z. M. Ye, Z. W. Cai, Y. L. Chang, S. F. Wang, Q. H. Gong and Y. F. Liu, *Adv. Mater*., 2010, **22**, 103.
91 L. Jia, D. H. Wang, Y. X. Huang, A. W. Xu and H. Q. Yu, *J. Phys. Chem. C*, 2011, **115**, 11466.
92 Q. Li, B. D. Guo, J. G. Yu, J. R. Ran, B. H. Zhang, H. J. Yan and J. R. Gong, *J. Am. Chem. Soc*., 2011, **133**, 10878.
93 J. L. Wu, S. Bai, X. P. Shen and L. Jiang, *Appl. Surf. Sci*., 2010, **257**, 747.
94 X. M. Geng, L. Niu, Z. Y. Xing, R. S. Song, G. T. Liu, M. T. Sun, G. S. Cheng, H. J. Zhong, Z. H. Liu, Z. J. Zhang, L. F. Sun, H. X. Xu, L. Lu and L. W. Liu, *Adv. Mater*., 2010, **22**, 638.
95 E. P. Gao, W. Z. Wang, M. Shang and J. H. Xu, *Phys. Chem. Chem. Phys*., 2011, **13**, 2887.
96 A. Mukherji, B. Seger, G. Q. Lu and L. Z. Wang, *ACS Nano*, 2011, **5**, 3483.
97 Y. S. Fu and X. Wang, *Ind. Eng. Chem. Res*., 2011, **50**, 7210.
98 X. F. Zhang, X. Quan, S. Chen and H. T. Yu, *Appl. Catal., B*, 2011, **105**, 237.
99 F. Zhou, R. Shi and Y. F. Zhu, *J. Mol. Catal. A: Chem*., 2011, **340**, 77.
100 Y. Q. Sun, C. Li, Y. X. Xu, H. Bai, Z. Y. Yao and G. Q. Shi, *Chem. Commun*., 2010, **46**, 4740.
101 Q. J. Xiang, J. G. Yu and M. Jaroniec, *J. Phys. Chem. C*, 2011, **115**, 7355.
102 H. Zhang, X. F. Fan, X. Quan, S. Chen and H. T. Yu, *Environ. Sci. Technol*., 2011, **45**, 5731.
103 M. S. Zhu, P. L. Chen and M. H. Liu, *ACS Nano*, 2011, **5**, 4529.
104 T. N. Lambert, C. A. Chavez, B. Hernandez-Sanchez, P. Lu, N. S. Bell, A. Ambrosini, T. Friedman, T. J. Boyle, D. R. Wheeler and D. L. Huber, *J. Phys. Chem. C*, 2009, **113**, 19812.
105 N. Li, G. Liu, C. Zhen, F. Li, L. L. Zhang and H. M. Cheng, *Adv. Funct. Mater*., 2011, **21**, 1717.
106 D. H. Wang, D. W. Choi, J. Li, Z. G. Yang, Z. M. Nie, R. Kou, D. H. Hu, C. M. Wang, L. V. Saraf, J. G. Zhang, I. A. Aksay and J. Liu, *ACS Nano*, 2009, **3**, 907.
107 Y. Park, S. H. Kang and W. Choi, *Phys. Chem. Chem. Phys*., 2011, **13**, 9425.
108 J. Du, X. Y. Lai, N. L. Yang, J. Zhai, D. Kisailus, F. B. Su, D. Wang and L. Jiang, *ACS Nano*, 2011, **5**, 590.
109 C. Z. Zhu, S. J. Guo, P. Wang, L. Xing, Y. X. Fang, Y. M. Zhai and S. J. Dong, *Chem. Commun*., 2010, **46**, 7148.
110 J. S. Chen, Z. Y. Wang, X. C. Dong, P. Chen and X. W. Lou, *Nanoscale*, 2011, **3**, 2158.
111 N. J. Bell, H. N. Yun, A. J. Du, H. Coster, S. C. Smith and R. Amal, *J. Phys. Chem. C*, 2011, **115**, 6004.
112 O. Akhavan and E. Ghaderi, *J. Phys. Chem. C*, 2009, **113**, 20214.
113 S. M. Paek, E. Yoo and I. Honma, *Nano Lett*., 2009, **9**, 72.
114 S. J. Ding, J. S. Chen, D. Y. Luan, F. Y. C. Boey, S. Madhavi and X. W. Lou, *Chem. Commun*., 2011, **47**, 5780.
115 P. Wang, Y. M. Zhai, D. J. Wang and S. J. Dong, *Nanoscale*, 2011, **3**, 1640.
116 J. F. Shen, B. Yan, M. Shi, H. W. Ma, N. Li and M. X. Ye, *J. Mater. Chem*., 2011, **21**, 3415.
117 O. Carp, C. L. Huisman and A. Reller, *Prog. Solid State Chem*., 2004, **32**, 33.
118 X. L. Hu, G. S. Li and J. C. Yu, *Langmuir*, 2010, **26**, 3031.
119 C. H. Li, F. Wang and J. C. Yu, *Energy Environ. Sci*., 2011, **4**, 100.
120 Q. J. Xiang, J. G. Yu and P. K. Wong, *J. Colloid Interface Sci*., 2011, **357**, 163.
121 G. Liu, H. G. Yang, X. W. Wang, L. N. Cheng, J. Pan, G. Q. Lu and H. M. Cheng, *J. Am. Chem. Soc*., 2009, **131**, 12868.
122 J. G. Yu, G. P. Dai, Q. J. Xiang and M. Jaroniec, *J. Mater. Chem*., 2011, **21**, 1049.
123 (*a*) J. G. Yu, T. T. Ma and S. W. Liu, *Phys. Chem. Chem. Phys*., 2011, **13**, 3491; (*b*) J. G. Yu, T. T. Ma, G. Liu and B. Cheng, *Dalton Trans*., 2011, **40**(25), 6635; (*c*) J. G. Yu, J. J. Fan and B. Cheng, *J. Power Sources*, 2011, **196**, 7891.
124 S. X. Min and G. X. Lu, *J. Phys. Chem. C*, 2011, **115**, 13938.
125 F. Wang and K. Zhang, *J. Mol. Catal. A: Chem*., 2011, **345**, 101.
126 C. Park, E. S. Engel, A. Crowe, T. R. Gilbert and N. M. Rodriguez, *Langmuir*, 2000, **16**, 8050.
127 L. L. Zhang, Z. G. Xiong and X. S. Zhao, *ACS Nano*, 2010, **4**, 7030.
128 Y. H. Zhang, Z. R. Tang, X. Z. Fu and Y. J. Xu, *ACS Nano*, 2010, **4**, 7303.

129 J. C. Liu, H. W. Bai, Y. J. Wang, Z. Y. Liu, X. W. Zhang and D. D. Sun, *Adv. Funct. Mater.*, 2010, **20**, 4175.
130 K. F. Zhou, Y. H. Zhu, X. L. Yang, X. Jiang and C. Z. Li, *New J. Chem.*, 2011, **35**, 353.
131 C. Chen, W. M. Cai, M. C. Long, B. X. Zhou, Y. H. Wu, D. Y. Wu and Y. J. Feng, *ACS Nano*, 2010, **4**, 6425.
132 H. J. Zhang, P. P. Xu, G. D. Du, Z. W. Chen, K. Oh, D. Y. Pan and Z. Jiao, *Nano Res.*, 2011, **4**, 274.
133 T. Kamegawa, D. Yamahana and H. Yamashita, *J. Phys. Chem. C*, 2010, **114**, 15049.
134 Y. Y. Liang, H. L. Wang, H. S. Casalongue, Z. Chen and H. J. Dai, *Nano Res.*, 2010, **3**, 701.
135 W. Q. Fan, Q. H. Lai, Q. H. Zhang and Y. Wang, *J. Phys. Chem. C*, 2011, **115**, 10694.
136 X. Y. Zhang, H. P. Li, X. L. Cui and Y. H. Lin, *J. Mater. Chem.*, 2010, **20**, 2801.
137 J. G. Yu, J. C. Yu, M. K. P. Leung, W. K. Ho, B. Cheng, X. J. Zhao and J. C. Zhao, *J. Catal.*, 2003, **217**, 69.
138 J. G. Yu, W. G. Wang, B. Cheng and B. L. Su, *J. Phys. Chem. C*, 2009, **113**, 6743.
139 J. G. Yu, L. J. Zhang, B. Cheng and Y. R. Su, *J. Phys. Chem. C*, 2007, **111**, 10582.
140 J. C. Yu, W. K. Ho, J. G. Yu, H. Yip, P. K. Wong and J. C. Zhao, *Environ. Sci. Technol.*, 2005, **39**, 1175.
141 J. G. Yu, Y. R. Su and B. Cheng, *Adv. Funct. Mater.*, 2007, **17**, 1984.
142 B. Cheng, Y. Le and J. G. Yu, *J. Hazard. Mater.*, 2010, **177**, 971.
143 J. G. Yu, G. P. Dai and B. B. Huang, *J. Phys. Chem. C*, 2009, **113**, 16394.
144 J. G. Yu, Q. J. Xiang, J. R. Ran and S. Mann, *CrystEngComm*, 2010, **12**, 872.
145 Y. H. Hu, H. Wang and B. Hu, *ChemSusChem*, 2010, **3**, 782.
146 S. J. Guo and S. J. Dong, *Chem. Soc. Rev.*, 2011, **40**, 2644.
147 H. X. Chang, X. J. Lv, H. Zhang and J. H. Li, *Electrochem. Commun.*, 2010, **12**, 483.
148 J. D. Roy-Mayhew, D. J. Bozym, C. Punckt and I. A. Aksay, *ACS Nano*, 2010, **4**, 6203.
149 L. Kavan, J. H. Yum and M. Gratzel, *ACS Nano*, 2011, **5**, 165.
150 H. T. Li, X. D. He, Z. H. Kang, H. Huang, Y. Liu, J. L. Liu, S. Y. Lian, C. H. A. Tsang, X. B. Yang and S. T. Lee, *Angew. Chem., Int. Ed.*, 2010, **49**, 4430.
151 D. H. Yoo, V. C. Tran, V. H. Pham, J. S. Chung, N. T. Khoa, E. J. Kim and S. H. Hahn, *Curr. Appl. Phys.*, 2011, **11**, 805.
152 J. C. Liu, L. Liu, H. W. Bai, Y. J. Wang and D. D. Sun, *Appl. Catal., B*, 2011, **106**, 76.
153 (*a*) J. G. Yu and J. R. Ran, *Energy Environ. Sci.*, 2011, **4**, 1364; (*b*) L. F. Qi, J. G. Yu and M. Jaroniec, *Phys. Chem. Chem. Phys.*, 2011, **13**, 8915.
154 J. G. Yu, Y. Hai and M. Jaroniec, *J. Colloid Interface Sci.*, 2011, **357**, 223.
155 X. Y. Zhang, Y. J. Sun, X. L. Cui and Z. Y. Jiang, *Int. J. Hydrogen Energy*, 2011, DOI: 10.1016/j.ijhydene.2011.04.053.
156 X. Y. Zhang, H. P. Li and X. L. Cui, *Chin. J. Inorg. Chem.*, 2009, **25**, 1903.
157 X. C. Wang, K. Maeda, A. Thomas, K. Takanabe, G. Xin, K. Domen and M. Antonietti, *Nat. Mater.*, 2009, **8**, 76.
158 T. F. Yeh, J. M. Syu, C. Cheng, T. H. Chang and H. S. Teng, *Adv. Funct. Mater.*, 2010, **20**, 2255.